Research Article Vol. 29, No. 4 / 15 February 2021 / Optics Express 5437
Optics EXPRESS

Switchable dual-band to broadband terahertz metamaterial absorber incorporating a VO_2 phase transition

TINGTING LV,[1,2] GUOHUA DONG,[1] CHUNHUA QIN,[1] JIA QU,[3,4] BO LV,[1] WENJIA LI,[1] ZHENG ZHU,[1] YUXIANG LI,[1] CHUNYING GUAN,[1] AND JINHUI SHI[1,5]

[1] *Key Laboratory of In-Fiber Integrated Optics of Ministry of Education, College of Physics and Optoelectronic Engineering, Harbin Engineering University, Harbin 150001, China*
[2] *School of Physics and Electronic Engineering, Northeast Petroleum University, Daqing 163318, China*
[3] *College of Aerospace and Civil Engineering, Harbin Engineering University, Harbin 150001, China*
[4] *qujia@hrbeu.edu.cn*
[5] *shijinhui@hrbeu.edu.cn*

Abstract: We design and demonstrate a thermally switchable terahertz metamaterial absorber consisting of an array of orthogonal coupled split-ring metal resonators involving a VO_2 phase transition. Numerical results indicate that the active metamaterial always absorbs the TE wave in dual-band regardless of insulating and metallic VO_2, while the insulator-to-metal phase transition enables a switchable effect between dual-band and broadband absorption of the TM wave with the resonant frequency tunability of 33%. Especially under the metallic VO_2 state, the absorption properties are polarization-dependent and exhibit a switching effect between dual-band and broadband absorption with the increase of the polarization angle. The tunable absorption mechanism can be explained by effective impedance theory and electric energy density distributions. The proposed dual-band to broadband metamaterial switching absorber may have broad applications in sensors, imaging and emitters.

1. Introduction

Metamaterial absorbers have drawn great interest due to their promise for potential applications such as solar-thermal energy harvesting [1], imaging [2] and sensors [3]. Landy et al. [4] firstly proposed a near unity absorbance metamaterial absorber by creating the impedance-matched between metamaterial and free space in the microwave frequency, and the structure design strategy gradually evolved into typical sandwiched configuration that comprised a layer of metallic resonators and a continuous ground plane separated by a dielectric spacer [5]. However, metamaterial absorbers are usually narrow-bandwidth or single-frequency absorption resulting from strong dispersion nature of resonance, which largely confines to their practical applications. To construct multiband and broadband metamaterial absorbers, the effective approaches are widely investigated based on lumped elements [6,7], doped silicon [8–10], graphene [11–13], black phosphorus [14], Mie resonance [15–16], destructive interference [17] and multiple resonance [18–30]. Among them, a simple and direct manner is multiple resonance, which refers to combining different resonators into hybrid metamaterial structure to broaden the absorption bandwidth. Judiciously stacking multiple vertically metallic layers or superposing coplanar sub-unit resonators can realize dual-band, triple-band, six-band and broadband absorbers based on the concept of the design. Fang et al. demonstrated an ultra-broadband absorber with the full absorption width at half-maximum (FWHM) of 86% based on 20-layer gradient sawteeth structure [19]. However, this scheme has certain limitations that the multilayer absorber design will increase the total thickness and the difficulty of fabrication. It is well known that the thickness

#418020 https://doi.org/10.1364/OE.418020
Journal © 2021 Received 18 Dec 2020; revised 27 Jan 2021; accepted 27 Jan 2021; published 4 Feb 2021

Optics EXPRESS

is a key factor in the practical integration of nanophotonic devices. Coplanar resonators design is an alternative approach to implement a simplified broadband absorber.

Since multiband and broadband absorption properties are very desirable, it would also be beneficial to dynamically tune and switch metamaterial absorber response by means of external stimuli. There has been considerable effort to achieve tunable metamaterial absorber involving phase transition material [31–34], solid state plasma [35], graphene [3,36–38], liquid crystal [39] or strontium titanate [40,41]. For instance, Mou et al. demonstrated a broadband and tunable absorber based on $Ge_2Sb_2Te_5$ (GST) for both visible and near-infrared waves, while the expansion of absorption bandwidth is achieved at the expense of the peak absorption [32]. The switching between two broadband terahertz absorber behaviors in six-layer metamaterial can be realized by controlling the phase transition of VO_2 [34]. Yao et al. proposed a dual-band wavelength-tunable graphene-based terahertz metamaterial absorber [37]. An all-dielectric H-shaped metamaterial was fabricated to exhibit tunable ultra-broadband terahertz absorption with a large frequency blueshift by 420 GHz [42]. While the majority of the reported tunable metamaterial absorbers are focused on the modulation of multiband to multiband and broadband to broadband, in which the metamaterials are always polarization insensitive. Polarization-dependent multiband to broadband tunability with near unity absorbance has seldom been explored in a thin terahertz metamaterial absorber. Tunable polarization-dependent metamaterial absorbers deserve much consideration since they are highly desirable in various applications such as thermal switching, polarization manipulation and energy harvesting.

In this work, we demonstrate a thermally switchable polarization-dependent metamaterial absorber in the terahertz frequency regime. The proposed metamaterial is consisted of an array of orthogonal coupled split-ring resonators (CSRR) with embedded VO_2 inclusions at different gaps. This hybrid design and asymmetric VO_2 pads arrangement provide a new freedom to flexibly tune absorption bandwidth and dynamic range by controlling an external thermal stimulus. At normal incidence, the metamaterial absorber always sustains dual-band absorption property for transverse electric (TE) polarization while exhibits dual-band to broadband switching performance for transverse magnetic (TM) polarization when the metamaterial experiences an insulator-to-metal phase transition of VO_2. Remarkably, the broadband absorber ($\sim$ 220 GHz bandwidth) can be accomplished with an absorption higher than 95.4% under the metallic VO_2 state. The dual-band absorbers are polarization insensitive and remain high absorption across a wide range of incident angles under the insulating VO_2 state. Such dual-band to broadband switchable terahertz metamaterial absorber is definitely beneficial to diverse potential applications in sensors, imaging and emitters, even can be extended to camouflage coating [43,44].

2. Discussion and results

The phase transition materials are helpful to create dynamic responses of metamaterial absorbers. Among them, vanadium dioxide (VO_2) is an excellent candidate due to the drastic insulator-to-metal phase transition at a threshold temperature of around 68°C. The conductivity change of VO_2 is as large as four or five orders of magnitude together with a reversible lattice structure transformation from a monoclinic to a tetragonal state during the phase transition. The phase transition process is fairly rapid since the switching time is on the order of picosecond, which shows promising for the application of high modulation speed. As a result, metamaterials with VO_2 inclusions provide an opportunity to realize tunable filter and tunable absorber [45–47]. Manipulating tunable absorption properties of terahertz wave is more attractive as terahertz functional components are scarce. The coupled split-ring resonators (CSRR), as a building block of chiral metamaterial, have been judiciously designed to enforce asymmetric transmission for circular polarization [48,49]. Here, CSRRs integrated VO_2 are used to construct a tunable absorber showing polarization-dependent switchable effect. The proposed tunable absorber configuration is schematically shown in Fig. 1. It consists of 90°-twisted CSRR patterns with

Optics EXPRESS

integrated VO_2 pads in different gaps and a continuous aluminum ground plane, which are separated by a polyimide dielectric layer with the thickness of $t = 22\mu m$. The unit cell of two 90°-twisted CSRRs is equivalent to a combination of two orthogonal CSRRs with a distance of $d = 20\mu m$. Their structural parameters are identical except for the split positions of two embedded VO_2 pads. The parameters are $w = 10$ μm, $a = 100$ μm, $b = 50$ μm, $c = 70$ μm and $s = 15$ μm, as shown in Fig. 1(b). The parameter s is split width, i.e. the length of the VO_2 pad. The tunable terahertz responses of the metamaterial are studied by commercial software CST Microwave Studio. Here, both of the CSRR and the metal layer are $t_m = 200$ nm thick aluminum with a conductivity of 3.56×10^7 S/m, and the thickness of VO_2 is the same as that of the CSRR. The polyimide layer can be regarded as a lossy dielectric with $\varepsilon_r = 3 + 0.09i$ (its loss tangent tan $\delta = 0.03$). The VO_2 material experiences an insulator to metal phase transition at ~68°C. The variable conductivities of VO_2 can be utilized to study the responses of the terahertz metamaterial to different temperatures [31,33,34]. In the insulating state, the dielectric constant of VO_2 in the terahertz regime is about 9 and its conductivity is smaller than 200 S/m, and in the metallic state the conductivity of VO_2 is as high as an order of 10^5 S/m [50–52]. In the simulation, the periodic boundaries are defined along both x and y directions, and the open boundary is applied along the z direction. Given that the transmittance is nearly zero due to the presence of a metal ground layer, the absorption (A) is extracted by the equation $A = 1 - R$, in which R denotes the reflectance of the metamaterial structure. The perfect absorption can be simply acquired by minimizing the reflectance.

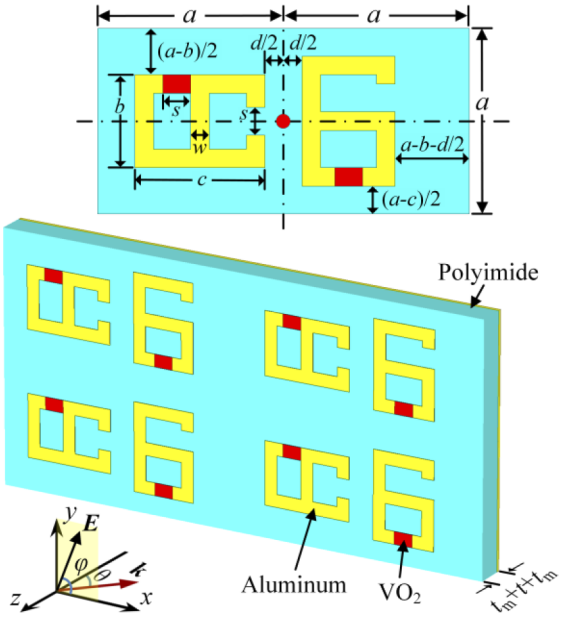

Fig. 1. The structural schematic of the proposed switchable metamaterial absorber with integrated VO_2 phase material. The red dot locates the geometrical center of the unit cell. The polarization angle φ and incident angle θ are marked in the inset.

The absorption spectra of the CSRR metamaterial with VO_2 phase transition are shown in Fig. 2 for forward (-z) normally propagating TM and TE wave excitation, in which TM and TE waves are defined as their magnetic and electric fields parallel to the y direction, respectively. The phase states of VO_2 layer at different temperatures can be modeled with the conductivity σ_V, in which the conductivity values 200 S/m and 10^5 S/m correspond to the complete insulating and metallic phases, respectively. When the metamaterial is illuminated by incident TM wave,

Optics EXPRESS

a clear evolution from dual-band to broadband absorption is presented as shown in Fig. 2(a) in the process of insulator-to-metal transition. When VO_2 is in the complete insulating state with $\sigma_V = 200$ S/m at the temperature of approximate 25°C, two distinct absorption peaks with efficiencies of 99% and 97.8% occur at the frequencies of $f_{I,1} = 0.67$ and $f_{I,2} = 0.87$ THz. With the increasing conductivity of the VO_2 pad, both the absorption values progressively weaken while the resonance peaks 1st and 2nd almost remain unchanged. When σ_V reaches 60000 S/m, the two absorption peaks in lower frequencies is in the "OFF" state, and a flat absorption spectrum emerges at higher frequencies. As σ_V further increases, the absorption values are about 98.7% and 99.3% at $f_{M,1} = 0.94$ and $f_{M,2} = 1.1$ THz [seen in Fig. 3(c)]. The minimal absorption is larger than 95.4% within a bandwidth of 220 GHz, superior to the reported switchable VO_2-based metamaterial absorber with over 90% absorption in ~100 GHz bandwidth [34]. The resonance frequency shift can be understood as the change of the resonance frequency during the phase transition, here in this two resonant absorption spectrum the value is given by $(\Delta f_1 + \Delta f_2)/2$, in which $\Delta f_1 = f_{M,1} - f_{I,1}$ and $\Delta f_2 = f_{M,2} - f_{I,2}$. The ratio of the resonance frequency shift is defined as $(\Delta f_1 / f_{I,1} + \Delta f_2 / f_{I,2})/2$. Especially, the THz metamaterial absorber is switched thermally from dual-band to broadband, the ratio of the resonance frequency shift is about 33% and the resonance frequency shift is about 250 GHz when the phase transition of VO_2 occurs from the insulating to metallic state. Although the resonance frequency shift of the proposed switchable absorber is less than that of all-dielectric H-shaped metamaterial, the thickness of our ultrathin metamaterial is around 1/16 times that of all-dielectric absorber [42]. For the case of incident TE polarization shown in Fig. 2(b), during the phase transition the proposed absorber always exhibits dual-band absorption of over 99.9% and 97.7%, and both the 1st and 2nd resonant frequencies have slight redshifts.

The tunable polarization-dependent absorption in the metamaterial can be understood according to resonant modes in Figs. 2(c) and 2(d). The spatial locations of integrated VO_2 can be appropriately selected to yield different absorption of TE and TM waves during the insulator-to-metal transition. The absorption spectra of TE and TM waves are nearly identical when VO_2 is insulating, however their electric field distributions are quite different. The electric fields of TM wave at both the resonant frequencies are mainly concentrated around the gaps with integrated VO_2 in Fig. 2(c) while those of TE wave are mainly concentrated around the air gaps in Fig. 2(d). The distribution of the field indicates that the electric-harmonic oscillators are formed. The equivalent circuits of the oscillators are composed of the inductors and capacitors and the resonant frequencies can be calculated as $f_{1,2} = 1/(2\pi(LC)^{1/2})$. The equivalent capacitors and inductors of the circuits are generated from the gaps and the metal strips of the split rings, as shown in Figs. 2(c) and 2(d). When the electric specification of the VO_2 changes from insulator to metal, the values of equivalent inductors reduce because the parallel-metal ribbons occur. Thus, the resonant frequencies become higher and the absorption spectra reveal redshift. Since the electric field almost distributes around the gaps with integrated VO_2 for TM wave illumination, the corresponding absorption spectrum exhibits a giant redshift.

To elucidate the absorption mechanism of the tunable absorber, the effective impedances of the metamaterial for incident TM wave are derived according to S parameter retrieval method [53]. The relative impedance of the metamaterial absorber can be denoted

$$z = \sqrt{\frac{(1+S_{11})^2 - (S_{21})^2}{(1-S_{11})^2 - (S_{21})^2}} = \frac{1+S_{11}}{1-S_{11}}$$

The condition of $Z = 1$ ($\mathrm{Re}(z) = 1$ and $\mathrm{Im}(z) = 0$) implies the perfect absorption can be achieved based on impedance match theory. As illustrated in Figs. 3(b) and 3(d), the real part of the effective impedance is close to 1 and the imaginary part approaches 0 at dual-band resonant frequencies and broadband region. Thus the impedance of the metamaterial is almost matched to free space.

Optics EXPRESS

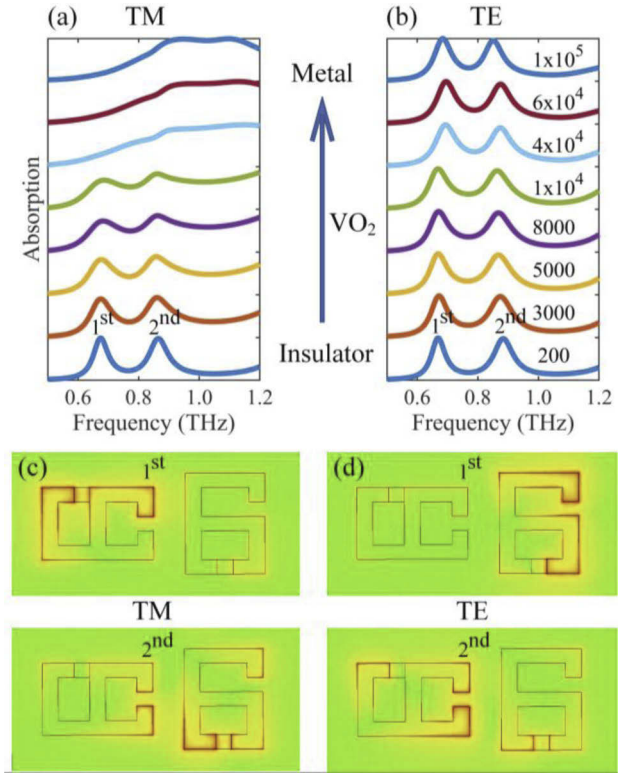

Fig. 2. Simulated polarization-dependent absorption spectra of the thermally controlled metamaterial at normal incidence. The absorption is presented as a function of conductivity of VO_2, indicating the insulator-to-metal phase transition. The electric field distributions of the metamaterial with insulating VO_2 are presented. (a)-(c) TM and (b)-(d) TE wave excitation.

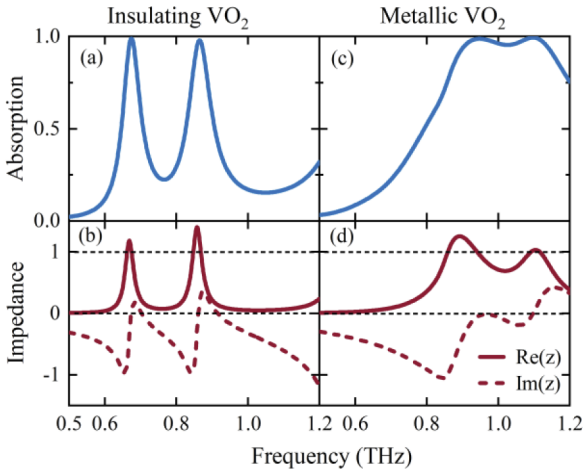

Fig. 3. The switching absorption properties of the metamaterial with insulator-to-metal phase transition for incident TM wave. (a), (c) Absorption spectra and (b), (d) the retrieved effective impedance of the tunable metamaterial absorber in the complete (a), (b) insulating and (b), (d) metallic states for incident TM polarization wave.

Optics EXPRESS

Wide-angle perfect metamaterial absorbers are conducive to practical applications. The angular and polarization dependence of tunable absorption are further investigated as illustrated in Fig. 4. For the CSRR metamaterial absorber with insulating VO_2, as shown in Figs. 4(a) and 4(c), the absorption spectrum below 1 THz is always dual-band and wide angle regardless of polarization. The low-frequency absorption peak is almost kept unmoved while the high-frequency one reveals slight red shift when the angle of incidence increases. Dual-band absorption property of the metamaterial for incident TM wave is robust and larger than 95% across a wide range of incident angle up to 80°, while for incident TE wave the dual-band absorption phenomenon exceeds 90% until the angle of incidence approaches $\theta = 45°$. Exceeding these angles, the intensities at absorption peaks of both TM and TE waves slowly fall. When VO_2 experiences an insulator-to-metal phase transition, the metamaterial still remains wide-angle dual-band absorption for incident TE wave in Fig. 4(b) while for TM wave the metamaterial exhibits broadband absorption instead of dual-band property at normal incidence as illustrated in Fig. 4(d). Dual-band performance of TE mode maintains high absorption intensity over 90% within a wide range of incident angle up to 55° in Fig. 4(b). In Fig. 4(d), the broadband absorption feature is accessible when the angle of incidence is less than 30° and then the oblique incidence leads to attenuation and split of broadband absorption. Specially, the metamaterial with metallic VO_2 also exhibits a broadband absorption of over 99% with a maximum bandwidth of 50 GHz in the range of 45°- 65°. Next, the effect of the polarization angle on the switchable absorption will be studied. For simplicity, the normal incidence is always kept unchanged when the effect of the polarization angle is investigated. When the VO_2 is in the insulating state in Fig. 4(e), the polarization angle hardly impacts on the efficiency of the dual-band absorption as well as the resonant frequencies and the absorption is always larger than 93%. As the VO_2 is in the metallic

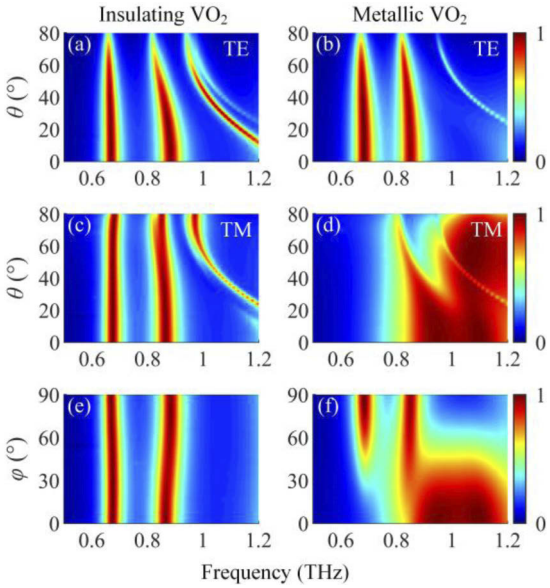

Fig. 4. Dual-band and broadband absorption performance of the tunable metamaterial as a function of polarization angle φ and incident angle θ. (a) and (b) Absorption of the metamaterial for incident TE wave at different angles, with insulating and metallic VO_2 respectively. (c) and (d) Absorption of the metamaterial for incident TM wave at different angles, with insulating and metallic VO_2 respectively. (e) and (f) Absorption of the metamaterial as a function of polarization angle φ at normal incidence, with insulating and metallic VO_2 respectively.

Optics EXPRESS

state in Fig. 4(f), the polarization angle enables the switching effect between dual-band and broadband absorption. Both dual-band and broadband absorption spectra achieve peak values greater than 90% in the range of 0°-20° and 70°-90°. The transition between dual-band and broadband absorption occurs around 45°. It's worth noting that additional absorption peaks together with strong angular dispersion can be observed, resulting from the high-order resonances at higher frequencies for larger angles of incidence [54, 55].

The aforementioned results show that the active metamaterial always absorbs TE wave in dual-band regardless of insulating and metallic VO_2 while the insulator-to-metal phase transition enables a switchable effect between dual-band and broadband absorption of TM wave. Undoubtedly, it is necessary to understand the switching phenomenon of TM wave absorption that is induced by the insulator-to-metal phase transition of VO_2 inclusion. In order to explore physical insight into the tunable absorption mechanism, the electric energy density (absorption) distributions of hybrid CSRRs with integrated VO_2 pads are calculated and the two cases of the insulating and metallic VO_2 are presented in Figs. 5 and 6, respectively. Different density distributions at 0.67 THz and 0.87 THz are presented as shown in Figs. 5(a) and 5(b). The density distribution in the lower frequency is mainly confined in the upper part of the CSRR on the left, indicating that the absorption mode is individually dominated by the left CSRR structure. For the high frequency absorption, the strongest absorption takes place around the right part of the left CSRR and the bottom part of the right CSRR, thus the hybrid CSRRs with integrated VO_2 pads contribute together to the absorption mode. When the VO_2 is in the metallic state, the metamaterial exhibits a broadband absorption spectrum with three resonances in Fig. 6. Most of the power absorption at 0.94 THz occurs in the left CSRR in Fig. 6(a). At 1.10 THz, most of the power absorption occurs in the right CSRR in Fig. 6(c). For the intermediate absorption dip at 1.03 THz, the absorption happens in both left and right CSRRs. As a result, the insulator-to-metal phase transition of VO_2 leads to variation of resonant modes, which contributes to the switching property of TM absorption spectrum.

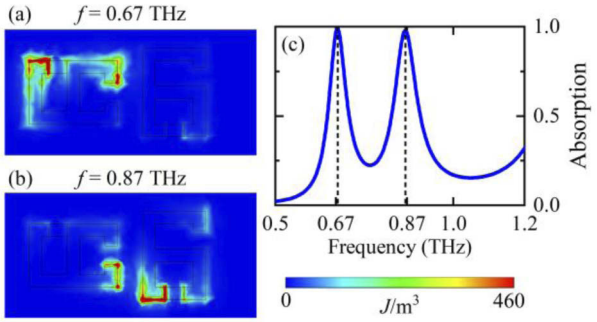

Fig. 5. Electric energy density distributions at (a) 0.67 THz and (b) 0.87 THz. (c) The dual-band absorption spectrum of the metamaterial with the insulating VO_2 for TM polarization incidence.

The effects of the structural parameters on tunable absorption performance are investigated in terms of TM wave incidence. Figures 7(a), 7(c) and 7(e) show the simulated results of the metamaterial with the insulating VO_2 as a function of the coupling distance *d,* split width *s* and the thickness *t* of dielectric layer. The distance *d* affects the coupling between the two orthogonal CSRRs and further influences the absorption properties. Dual-band absorption resonant frequencies and peak values are almost kept unmoved when the distance *d* is larger than 20μm in Fig. 7(a). It is also noted that the high-frequency resonance peak is more sensitive to the small distance than the low-frequency one. When the coupling distance is infinitely small ($d \rightarrow 0$), the two resonators are electrically connected and the resonant frequencies largely

Optics EXPRESS

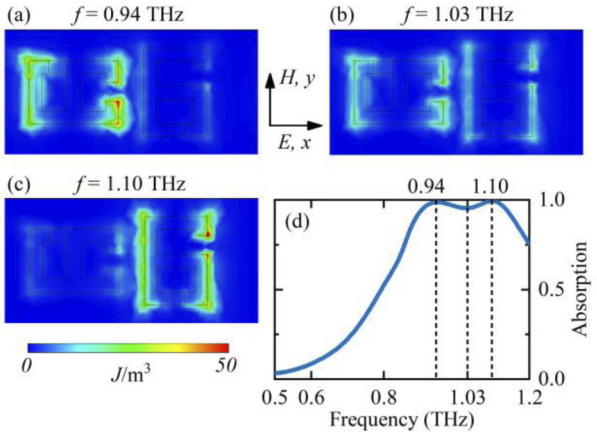

Fig. 6. Electric energy density distributions at (a) 0.94 THz, (b) 1.03 THz and (c) 1.10 THz. The broadband absorption spectrum of the metamaterial with the metallic VO_2 for TM polarization incidence.

shift, where the metamaterial absorbs most energy. Considering the split width s (the length of VO_2), the performance of the dual-band absorber almost maintains unchanged in Fig. 7(c), only accompanied by a distinct blue shift with the increase of s.

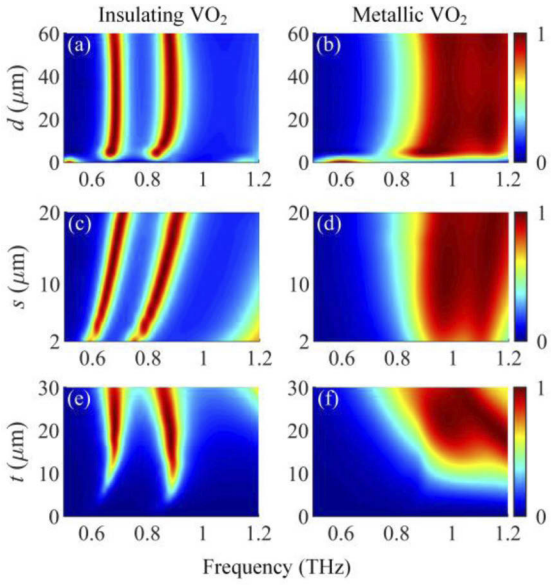

Fig. 7. Geometrical dependence of the switchable dual-band to broadband absorption properties in the hybrid metamaterial for TM polarization as a function of (a)-(b) the distance d between the coupled resonators, (c)-(d) the split gap s of embedded VO_2 pads and (e)-(f) the thickness of the dielectric layer t when the VO_2 is in the insulating or metallic phase, respectively. The only one parameter is variable while others are kept unchanged.

The dielectric layer thickness between the ground metal layer and the CSRRs is an important parameter. The appropriate dielectric thickness enables dual-band absorption performance while the dual-band absorption feature vanishes in Fig. 7(e) when the dielectric thickness is

Optics EXPRESS

less than 10μm. When the integrated VO_2 experiences an insulator-to-metal phase transition, parameters analyses of the metamaterial absorber are presented in Figs. 7(b), 7(d) and 7(f). Obviously, broadband absorption properties of the metamaterial with metallic VO_2 are robust within a relatively large parameter range, which is quite similar to that of the metamaterial with insulating VO_2. In Fig. 7(b), the broadband absorption spectrum abruptly red-shifts due to conductive coupling of two connected resonators when the coupling distance is infinite small ($d \rightarrow 0$). When the length s of VO_2 is in the range of 5-20 μm, the metamaterial fairly reveals broadband absorption in Fig. 7(d), while the absorption efficiency and its bandwidth deteriorate until the length s is less than 5 μm. Compared with the coupling distance d and the length s of VO_2, the dielectric thickness t more seriously impacts the absorption behavior no matter the VO_2 is insulating or metallic in Figs. 7(e) and 7(f). The bandwidth and absorption peaks strongly depend on the change of the dielectric layer thickness in Fig. 7(f). Taking account of both absorption intensity and bandwidth, the applicable parameters with $d = 20$ μm, $s = 15$ μm and $t = 22$ μm can be readily obtained. Meanwhile, the tunable absorption performance can be well engineered by adjusting the structural parameters.

Although the experimental verification of the proposed metamaterial has not been provided here, the proposed metamaterial can be readily fabricated by lithography and lift off technology [56,57]. The polyimide is flexible to be easily deformed, thus this metamaterial may cover on curved surfaces in conformal applications. The CSRR metamaterial can actively absorb electromagnetic wave or manipulate the polarization state by use of insulator-to-metal phase transition of VO_2. For instance, the metamaterial exhibits conductivity-dependent absorption around 1 THz when it is illuminated by TM wave in Fig. 2(a), thus the absorption can be thermally switched on/off. In addition, the CSRR metamaterial with VO_2 can manipulate the polarization state since it differently absorbs TE and TM waves during the phase transition as shown in Figs. 4(c) and 4(f).

3. Conclusion

In conclusion, we propose the numerical demonstration of a dual-band to broadband THz switchable absorber that consists of combined CSRR patterns with embedded VO_2-based phase transition. The broadband absorption spectrum is higher than 95.4% with an absorption bandwidth of 220 GHz, and the tunability of the resonant frequency is about 33% when the phase transition of VO_2 occurs from the insulating to metallic state. Especially, under the insulating VO_2 state, dual-band absorption properties are polarization-independent and robust over a wide angle of incidence around 45°. On the contrary, the absorption properties exhibit polarization-dependent with a dual-band to broadband switching effect that is induced by the insulator-to-metal phase transition of VO_2. The physical mechanism of the switchable absorption effect can be understood by effective impedance theory and electric energy density distributions. Further, the switchable absorption performance can be well engineered by adjusting the structural parameters. The proposed switchable metamaterial absorber has potential applications in sensors, imaging and emitters.

Funding. National Natural Science Foundation of China (U1931121, 61675054, 91750107); Natural Science Foundation of Heilongjiang Province (ZD2020F002, ZD2018015); 111 Project to Harbin Engineering University (B13015); Fundamental Research Funds for the Central Universities (3072020CF2528, 3072020CFT2501).

Acknowledgments. Thanks to the State Key Laboratory of Millimeter Waves of Southeast University.

Disclosures. The authors declare no conflicts of interest.

References

1. K.-T. Lin, H. Lin, T. S. Yang, and B. H. Jia, "Structured graphene metamaterial selective absorbers for high efficiency and omnidirectional solar thermal energy conversion," Nat. Commun. **11**, 1389 (2020).
2. X. L. Liu, T. Starr, A. F. Starr, and W. J. Padilla, "Infrared spatial and frequency selective metamaterial with near-unity absorbance," Phys. Rev. Lett. **104**, 207403 (2010).

Optics EXPRESS

3. M. S. Islam, J. Sultana, M. Biabanifard, Z. Vafapour, M. J. Nine, A. Dinovitser, C. M. B. Cordeiro, B. W.-H. Ng, and D. Abbott, "Tunable localized surface plasmon graphene metasurface for multiband superabsorption and terahertz sensing," Carbon **158**, 559–567 (2020).
4. N. I. Landy, S. Sajuyigbe, J. J. Mock, D. R. Smith, and W. J. Padilla, "Perfect metamaterial absorber," Phys. Rev. Lett. **100**, 207402 (2008).
5. H. Tao, C. M. Bingham, A. C. Strikwerda, D. Pilon, D. Shrekenhamer, N. I. Landy, K. Fan, X. Zhang, W. J. Padilla, and R. D. Averitt, "Highly flexible wide angle of incidence terahertz metamaterial absorber: Design, fabrication, and characterization," Phys. Rev. B **78**, 241103(R) (2008).
6. T. T. Nguyen and S. Lim, "Angle-and polarization-insensitive broadband metamaterial absorber using resistive fan-shaped resonators," Appl. Phys. Lett. **112**, 021605 (2018).
7. S. J. Li, J. Gao, X. Y. Cao, W. Q. Li, Z. Zhang, and D. Zhang, "Wideband, thin, and polarization-insensitive perfect absorber based the double octagonal rings metamaterials and lumped resistances," J. Appl. Phys. **116**, 043710 (2014).
8. M. B. Pu, M. Wang, C. G. Hu, C. Huang, Z. Y. Zhao, Y. Q. Wang, and X. G. Luo, "Engineering heavily doped silicon for broadband absorber in the terahertz regime," Opt. Express **20**, 25513–25519 (2012).
9. W. Withayachumnankul, C. M. Shah, C. Fumeaux, B. S.-Y. Ung, W. J. Padilla, M. Bhaskaran, D. Abbott, and S. Sriram, "Plasmonic resonance toward terahertz perfect absorbers," ACS Photonics **1**(7), 625–630 (2014).
10. S. Yin, J. F. Zhu, W. D. Xu, W. Jiang, J. Yuan, G. Yin, L. J. Xie, Y. B. Ying, and Y. G. Ma, "High-performance terahertz wave absorbers made of silicon-based metamaterials," Appl. Phys. Lett. **107**, 073903 (2015).
11. C. Liu, L. M. Qi, and X. Zhang, "Broadband graphene-based metamaterial absorbers," AIP Adv. **8**, 015301 (2018).
12. R. M. Gao, Z. C. Xu, C. F. Ding, L. Wu, and J. Q. Yao, "Graphene metamaterial for multiband and broadband terahertz absorber," Opt. Commun. **356**, 400–404 (2015).
13. Y. W. Deng, L. Peng, X. Liao, and X. Jiang, "An ultra-broadband terahertz absorber based on coplanar graphene and gold hybridized metasurface," Plasmonics **14**(5), 1057–1061 (2018).
14. Y. M. Qing, H. F. Ma, and T. J. Cui, "Tailoring anisotropic perfect absorption in monolayer black phosphorus by critical coupling at terahertz frequencies," Opt. Express **26**(25), 32442–32450 (2018).
15. X. M. Liu, C. W. Lan, B. Li, Q. Zhao, and J. Zhou, "Dual band metamaterial perfect absorber based on artificial dielectric "molecules"," Sci. Rep. **6**, 28906 (2016).
16. X. M. Liu, C. W. Lan, K. Bi, B. Li, Q. Zhao, and J. Zhou, "Dual band metamaterial perfect absorber based on Mie resonances," Appl. Phys. Lett. **109**, 062902 (2016).
17. J. B. Sun, L. Y. Liu, G. Y. Dong, and J. Zhou, "An extremely broad band metamaterial absorber based on destructive interference," Opt. Express **19**(22), 21155–21162 (2011).
18. X. P. Shen, T. J. Cui, J. M. Zhao, H. F. Ma, W. X. Jiang, and H. Li, "Polarization-independent wide-angle triple-band metamaterial absorber," Opt. Express **19**(10), 9401–9407 (2011).
19. Y. X. Cui, K. H. Fung, J. Xu, H. Ma, Y. Jin, S. L. He, and N. X. Fang, "Ultra-broadband light absorption by a sawtooth anisotropic metamaterial slab," Nano Lett. **12**(3), 1443–1447 (2012).
20. H. L. Huang, H. Xia, Z. B. Guo, D. Xie, and H. J. Li, "Design of broadband metamaterial absorbers for permittivity sensitivity and solar cell application," Chin. Phys. Lett. **34**(11), 117801 (2017).
21. C. Wu and G. Shvets, "Design of metamaterial surfaces with broadband absorbance," Opt. Lett. **37**(3), 308–310 (2012).
22. C. M. Tran, H. V. Pham, H. T. Nguyen, T. T. Nguyen, L. D. Vu, and T. H. Do, "Creating multiband and broadband metamaterial absorber by multiporous square layer structure," Plasmonics **14**(6), 1587–1592 (2019).
23. Y. J. Kim, Y. J. Yoo, K. W. Kim, J. Y. Rhee, Y. H. Kim, and Y. Lee, "Dual broadband metamaterial absorber," Opt. Express **23**(4), 3861–3868 (2015).
24. F. Ding, Y. X. Cui, X. C. Ge, F. Zhang, Y. Jin, and S. L. He, "Ultra-broadband microwave metamaterial absorber," Appl. Phys. Lett. **100**, 103506 (2012).
25. Y. M. Qing, H. F. Ma, S. Yu, and T. J. Cui, "Tunable dual-band perfect metamaterial absorber based on a graphene-SiC hybrid system by multiple resonance modes," J. Phys. D: Appl. Phys. **52**(1), 015104 (2018).
26. J. Sun, K. Chen, G. W. Ding, W. L. Guo, J. M. Zhao, Y. J. Feng, and T. Jiang, "Achieving directive radiation and broadband microwave absorption by an anisotropic metasurface," IEEE Access **7**, 93919–93926 (2019).
27. Y. Q. Ye, Y. Jin, and S. L. He, "Omnidirectional, polarization-insensitive and broadband thin absorber in the terahertz regime," J. Opt. Soc. Am. B **27**(3), 498–504 (2010).
28. B. X. Wang, G. Z. Wang, T. Sang, and L. L. Wang, "Six-band terahertz metamaterial absorber based on the combination of multiple-order responses of metallic patches in a dual-layer stacked resonance structure," Sci. Rep. **7**, 41373 (2017).
29. L. Huang, D. R. Chowdhury, S. Ramani, M. T. Reiten, S. N. Luo, A. J. Taylor, and H. T. Chen, "Experimental demonstration of terahertz metamaterial absorbers with a broad and flat high absorption band," Opt. Lett. **37**(2), 154–156 (2012).
30. X. J. He, S. T. Yan, Q. X. Ma, Q. F. Zhang, P. Jia, F. M. Wu, and J. X. Jiang, "Broadband and polarization-insensitive terahertz absorber based on multilayer metamaterials," Opt. Commun. **340**, 44–49 (2015).
31. Q. Y. Wen, H. W. Zhang, Q. H. Yang, Z. Chen, Y. Long, Y. L. Jing, Y. Lin, and P. X. Zhang, "A tunable hybrid metamaterial absorber based on vanadium oxide films," J. Phys. D: Appl. Phys. **45**, 235106 (2012).

Optics EXPRESS

32. N. L. Mou, X. L. Liu, T. Wei, H. X. Dong, Q. He, L. Zhou, Y. Q. Zhang, L. Zhang, and S. L. Sun, "Large-scale, low-cost, broadband and tunable perfect optical absorber based on phase change material," Nanoscale **12**, 5374–5379 (2020).
33. L. Lei, F. Lou, K. Y. Tao, H. X. Huang, X. Cheng, and P. Xu, "Tunable and scalable broadband metamaterial absorber involving VO_2-based phase transition," Photonics Res. **7**(7), 734–741 (2019).
34. Y. Zhao, Q. P. Huang, H. L. Cai, X. X. Lin, and Y. L. Lu, "A broadband and switchable VO_2-based perfect absorber at the THz frequency," Opt. Commun. **426**, 443–449 (2018).
35. X. R. Kong, H. F. Zhang, R. N. Dao, and G. B. Liu, "A tunable polarization insensitive ultra-broadband absorber based on the plasma metamaterial," Opt. Commun. **453**, 124435 (2019).
36. M. L. Huang, Y. Z. Cheng, Z. Z. Cheng, H. R. Chen, X. S. Mao, and R. Z. Gong, "Based on graphene tunable dual-band terahertz metamaterial absorber," Opt. Commun. **415**, 194–201 (2018).
37. G. Yao, F. R. Ling, J. Yue, C. Y. Luo, J. Ji, and J. Q. Yao, "Dual-band tunable perfect metamaterial absorber in the THz range," Opt. Express **24**, 1518–1527 (2016).
38. Y. P. Zhang, T. T. Li, Q. Chen, H. Y. Zhang, J. F. O'Hara, E. Abele, A. J. Taylor, H. T. Chen, and A. K. Azad, "Independently tunable dual-band perfect absorber based on graphene at mid-infrared frequencies," Sci. Rep. **5**, 18463 (2015).
39. D. Shrekenhamer, W. C. Chen, and W. J. Padilla, "Liquid crystal tunable metamaterial perfect absorber," Phys. Rev. Lett. **110**(17), 177403 (2013).
40. C. Y. Luo, Z. Z. Li, Z. H. Guo, J. Yue, Q. Luo, G. Yao, J. Ji, Y. K. Rao, R. K. Li, D. Li, H. X. Wang, J. Q. Yao, and F. R. Ling, "Tunable metamaterial dual-band terahertz absorber," Solid State Commun. **222**, 32–36 (2015).
41. W. Y. Li and Y. Z. Cheng, "Dual-band tunable terahertz perfect metamaterial absorber based on strontium titanate (STO) resonator structure," Opt. Commun. **462**, 125265 (2020).
42. X. G. Zhao, Y. Wang, J. Schalch, G. W. Duan, K. Cremin, J. D. Zhang, C. X. Chen, R. D. Averitt, and X. Zhang, "Optically modulated ultra-broadband all-silicon metamaterial terahertz absorbers," ACS Photonics **6**, 830−837 (2019).
43. J. C. Zhao, Y. Wang, Y. C. Zhu, W. Zhang, and Y. T. Yu, "Lithography-free flexible perfect broadband absorber in visible light based on an all-dielectric multilayer structure," Opt. Lett. **45**, 5464–5467 (2020).
44. F. Y. Dong, S. Xu, W. Guo, N. Jiang, D. Han, X. He, L. Zhang, Z. Wang, J. Feng, W. Su, and H. B. Sun, "Solar-energy camouflage coating with varying sheet resistance," Nano Energy **77**, 105095 (2020).
45. T. L. Wang, H. Y. Zhang, Y. Zhang, Y. P. Zhang, and M. Y. Cao, "Tunable bifunctional terahertz metamaterial device based on Dirac semimetals and vanadium dioxide," Opt. Express **28**(12), 17434–17448 (2020).
46. T. L. Wang, Y. P. Wang, H. Y. Zhang, and M. Y. Cao, "Dual-controlled switchable broadband terahertz absorber based on a graphene-vanadium dioxide metamaterial," Opt. Mater. Express **10**(2), 369–386 (2020).
47. W. J. Kang, Q. G. Gao, L. L. Dai, Y. L. Zhang, H. Y. Zhang, and Y. P. Zhang, "Dual-controlled tunable terahertz coherent perfect absorption using Dirac semimetal and vanadium dioxide," Results Phys. **19**, 103688 (2020).
48. R. Singh, E. Plum, C. Menzel, C. Rockstuhl, A. K. Azad, R. A. Cheville, F. Lederer, W. Zhang, and N. I. Zheludev, "Terahertz metamaterial with asymmetric transmission," Phys. Rev. B **80**, 153104 (2009).
49. Z. C. Li, W. W. Liu, H. Cheng, S. Q. Chen, and J. G. Tian, "Tunable dual-band asymmetric transmission for circularly polarized waves with graphene planar chiral metasurfaces," Opt. Lett. **41**, 3142–3145 (2016).
50. Y. H. Zhu, S. Vegesna, Y. Zhao, V. Kuryatkov, M. Holtz, Z. Y. Fan, M. Saed, and A. A. Bernussi, "Tunable dual-band terahertz metamaterial bandpass filters," Opt. Lett. **38**, 2382–2384 (2013).
51. Y. H. Zhu, Y. Zhao, M. Holtz, Z. Y. Fan, and A. A. Bernussi, "Effect of substrate orientation on terahertz optical transmission through VO_2 thin films and application to functional antireflection coatings," J. Opt. Soc. Am. B **29**(9), 2373–2376 (2012).
52. Y. Zhao, J. H. Lee, Y. H. Zhu, M. Nazari, C. H. Chen, H. Y. Wang, A. Bernussi, M. Holtz, and Z. Y. Fan, "Structural, electrical, and terahertz transmission properties of VO_2 thin films grown on c-, r-, and m-plane sapphire substrates," J. Appl. Phys. **111**, 053533 (2012).
53. D. R. Smith, D. C. Vier, T. Koschny, and C. M. Soukoulis, "Electromagnetic parameter retrieval from inhomogeneous metamaterials," Phys. Rev. E **71**, 036617 (2005).
54. M. Diem, T. Koschny, and C. M. Soukoulis, "Wide-angle perfect absorber/thermal emitter in the THz regime," Phys. Rev. B **79**, 033101 (2009).
55. J. Wang, Y. T. Chen, J. M. Hao, M. Yan, and M. Qiu, "Shape-dependent absorption characteristics of three-layered metamaterial absorbers at near-infrared," J. Appl. Phys. **109**, 074510 (2011).
56. S. Liu, A. Noor, L. L. Du, L. Zhang, Q. Xu, K. Luan, T. Q. Wang, Z. Tian, W. X. Tang, J. G. Han, W. L. Zhang, X. Y. Zhou, Q. Cheng, and T. J. Cui, "Anomalous refraction and nondiffractive Bessel-beam generation of terahertz waves through transmission-type coding metasurfaces," ACS Photonics **3**(10), 1968–1977 (2016).
57. M. Liu, Q. Xu, X. Y. Chen, E. Plum, H. Li, X. Q. Zhang, C. H. Zhang, C. W. Zou, J. G. Han, and W. L. Zhang, "Temperature-controlled asymmetric transmission of electromagnetic waves," Sci. Rep. **9**(1), 4097 (2019).